Examination of a Theoretical Model of Streaming Potential Coupling Coefficient

Luong, D.T.; Sprik, R.

DOI
10.1155/2014/471819
Publication date
2014
Document Version
Final published version
Published in
ISRN Geophysics

Hindawi Publishing Corporation
International Journal of Geophysics
Volume 2014, Article ID 471819, 12 pages
http://dx.doi.org/10.1155/2014/471819

Research Article

Examination of a Theoretical Model of Streaming Potential Coupling Coefficient

D. T. Luong and R. Sprik

Van der Waals-Zeeman Institute, University of Amsterdam, 1098 XH Amsterdam, The Netherlands

Correspondence should be addressed to D. T. Luong; d.t.luong@uva.nl

Received 21 February 2014; Revised 6 April 2014; Accepted 23 April 2014; Published 27 May 2014

Academic Editor: Michael S. Zhdanov

Seismoelectric effects and streaming potentials play an important role in geophysical applications. The key parameter for those phenomena is the streaming potential coupling coefficient, which is, for example, dependent on the zeta potential of the interface of the porous rocks. Comparison of an existing theoretical model to experimental data sets from available published data for streaming potentials has been performed. However, the existing experimental data sets are based on samples with dissimilar fluid conductivity, pH of pore fluid, temperature, and sample compositions. All those dissimilarities may cause the observed deviations. To critically assess the models, we have carried out streaming potential measurement as a function of electrolyte concentration and temperature for a set of well-defined consolidated samples. The results show that the existing theoretical model is not in good agreement with the experimental observations when varying the electrolyte concentration, especially at low electrolyte concentration. However, if we use a modified model in which the zeta potential is considered to be constant over the electrolyte concentration, the model fits the experimental data well in a whole range of concentration. Also, for temperature dependence, the comparison shows that the theoretical model is not fully adequate to describe the experimental data but does describe correctly the increasing trend of the coupling coefficient as function of temperature.

1. Introduction

Electrokinetic phenomena are induced by the relative motion between a fluid and a solid surface and are directly related to the existence of an electric double layer between the fluid and the solid surface. Of electrokinetic phenomena, streaming potential and seismoelectric effects play an important role in geophysical applications. For example, streaming potential is used to map subsurface flow and detect subsurface flow patterns in oil reservoirs [1]. Streaming potential is also used to monitor subsurface flow in geothermal areas and volcanoes [2–4]. Monitoring of Streaming Potential anomalies has been proposed as a means of predicting earthquakes [5, 6]. Seismoelectric and electroseismic effects have been developed in order to investigate oil and gas reservoirs [7], hydraulic reservoirs [8–10], and downhole seismoelectric imaging [11]. It should be noted that electrokinetic phenomena are not applicable for porous media totally saturated with oil. However, reservoir rocks are normally saturated with oil, salt water, and gas. The coupling coefficient of conversions between seismic waves and electromagnetic waves is a theoretically involved expression of frequency and Streaming Potential coupling coefficient [12].

The key parameter for electrokinetic phenomena is the Streaming Potential coupling coefficient and therefore the zeta potential [4]. Normally, the coupling coefficient is experimentally measured and the zeta potential is then deduced from that with knowledge of the electrical conductivity, viscosity, and electrical permittivity of the fluid. Glover et al. [13] developed a theoretical model to calculate the zeta potential and Streaming Potential coefficient of reservoir rocks and other porous media. By using reasonable values of input parameters that are supported by independent measurements or theory, the authors have obtained and compared the theoretical results to an experimental data set of 290 Streaming Potential coefficient measurements and 269 zeta

potential measurements using data from 29 publications. The comparison shows that the theoretical model can reproduce the main features of the experimental data.

However, the experimental data set was collected from different sources that may lead to a dissimilarity in fluid conductivity at the same pore fluid concentration (quality of deionized water used to make brine may be not the same), in pH of pore fluid (a big range of pH from 5.5 to 11), in temperature, and so forth. Some microstructure parameters that are needed for the model were also not given in the original publications. The zeta potential and surface conductance themselves may be also different from sample to sample [14]. Therefore, all of those dissimilarities could lead the experimental data to spread around the theoretically modeled graphs for a given set of material.

In this work we want to examine how well the model works for 20 consolidated samples with 7 different concentration NaCl solutions and 9 different temperatures. To do so, firstly the coupling coefficients and the zeta potentials were experimentally measured as a function of electrolyte concentration and temperature. Afterwards the model was used by taking fluid parameters, rock-fluid interface parameters already provided in [13], and rock microstructure parameters (porosity, permeability, and formation factor) measured by us for all the samples. The proton surface conductance was adjusted to fit the experimental data. The comparisons were carried out for each sample.

For electrolyte concentration dependence of the coupling coefficient, the comparison shows that the theoretical model is not in agreement with the experimental data, especially in low concentration range. However, if the zeta potential is considered to be constant over electrolyte concentration the model fits the experimental data very well in a whole range of concentrations. This leads to the suggestion that the formula of the zeta potential against electrolyte concentration in the model needs to be adjusted accordingly. Besides the model given in [13], we also use other empirical models from Pride and Morgan [15], Vinogradov et al. [16], Jaafar et al. [17], and Jouniaux and Ishido [18] to predict the Streaming Potential coupling coefficient as a function of electrolyte concentration. But none of them can fit experimental data at low electrolyte concentration. For temperature dependence of the coupling coefficient, we implemented a zeta potential offset to the model which improves the fit to experimental data. The comparison shows that the theoretical model does not fit the experimental data well but it can show the increase of coupling coefficient with increasing temperature as measured. The reason for that could be due to the variation of some input parameters describing the rock/fluid interface over temperature rather than being constant as assumed in the experiment and a possible process activated by temperature happening around 300 K.

This work is a continuation and extension of the earlier work [14] in which permeability dependence of Streaming Potential coupling coefficients for porous media with taking into account the difference in the zeta potential among samples and the change of surface conductance against electrolyte concentration was studied. This work includes five sections. Section 2 describes the theoretical background of the streaming potential including the calculation of Stern potential, zeta potential, surface conductance, and Streaming Potential coupling coefficient of porous media. Section 3 presents the experimental measurements. Section 4 contains the experimental results, discussion, and comparisons between the experimental data and the results of the theoretical model. Conclusions are provided in Section 5.

2. Theoretical Background of Streaming Potential

2.1. Streaming Potential Coupling Coefficient. The streaming current is created by the relative motion of the diffuse layer with respect to the solid surface induced by a fluid pressure drop over the channel and is directly related to the existence of an electric double layer (EDL) between the fluid and the solid surface (for more details, see [24]). This streaming current is then balanced by a conduction current, leading to the streaming potential. In a porous medium, the electric current density and the fluid flux are coupled, so fluids moving through porous media generate a streaming potential [25]. The streaming potential increases linearly with the fluid pressure difference that drives the fluid flow, provided that the flow remains laminar [26]. The steady state Streaming Potential coupling coefficient is defined when the total current density is zero as

$$C_S = \frac{\Delta V}{\Delta P} = \frac{\epsilon_r \epsilon_0 \zeta}{\eta \sigma_{\text{eff}}}, \tag{1}$$

where ΔV is the streaming potential, ΔP is the fluid pressure difference, ϵ_r is the relative permittivity of the fluid, ϵ_0 is the dielectric permittivity in vacuum (8.854×10^{-12} F/m), η is the dynamic viscosity of the fluid, ζ is the zeta potential, and σ_{eff} is the effective conductivity. The zeta potential is the electric potential on the shear plane when a part of the diffuse layer is transported by fluid flow (for more details, see [11, 27]). The effective conductivity includes the intrinsic fluid conductivity and the surface conductivity. If the fluid conductivity is much higher than the surface conductivity (the fluid conductivity is larger than 0.13 S/m or 0.01 M NaCl solution for our measurement as stated in [14]), the effective conductivity is approximately equal to the fluid conductivity, $\sigma_{\text{eff}} = \sigma_f$. Therefore, the coupling coefficient becomes the well-known Helmholtz-Smoluchowski equation:

$$C_S = \frac{\epsilon_r \epsilon_0 \zeta}{\eta \sigma_f}. \tag{2}$$

According to [14], (1) can be written as

$$C_S = \frac{\epsilon_r \epsilon_0 \zeta}{\eta \left(\sigma_f + 2\left(\Sigma_s / \sqrt{8Fk_o}\right)\right)}, \tag{3}$$

where σ_f is the fluid conductivity, Σ_s is the surface conductance, F is the formation factor, and k_o is the permeability of the porous medium. Equation (3) shows that, besides the zeta potential, fluid conductivity, and surface conductance,

the coupling coefficient also depends on the microstructure of porous media such as permeability, porosity, and tortuosity expressed via the formation factor.

To calculate the coupling coefficient, one needs to know (1) the zeta potential, (2) the fluid relative electric permittivity, (3) the fluid viscosity, (4) the fluid conductivity, and (5) the surface conduction as a function of electrolyte concentration and temperature as well as the rock microstructure parameters such as permeability and formation factor. All of those are theoretically presented in [13]. In (3), we just rewrite the key expressions for the zeta potential and the surface conduction.

2.2. Zeta Potential. The electrical potential distribution φ in the EDL has, approximately, an exponential distribution given in [13, 28, 29]

$$\varphi = \varphi_d \exp\left(-\frac{\chi}{\chi_d}\right), \tag{4}$$

where φ_d is the Stern potential (V) given by

$$\varphi_d = \frac{2k_bT}{3e} \ln\left(\frac{\sqrt{8\ \times 10^3 \epsilon_0 \epsilon_r k_b T N}\left(10^{-\mathrm{pH}} + K_{Me}C_f\right)}{2e\Gamma_s K_{(-)}} \times \left[\frac{C_f + 10^{-\mathrm{pH}} + 10^{\mathrm{pH}-pKw}}{\sqrt{C_f}}\right]\right), \tag{5}$$

and χ_d is the Debye length (m) given by

$$\chi_d = \sqrt{\frac{\epsilon_0 \epsilon_r k_b T}{2000 N e^2 C_f}}, \tag{6}$$

and χ is the distance from the mineral surface. Equation (4) is, in fact, the solution of the linearized Poisson-Boltzmann equation describing the electrostatic potential distribution in the electrical double layer and is called the Debye-Hückel approximation [12]. The zeta potential can then be calculated as

$$\zeta = \varphi_d \exp\left(-\frac{\chi_\zeta}{\chi_d}\right), \tag{7}$$

where $\chi_\zeta = 2.4 \times 10^{-10}$ m is the shear plane distance (the distance from the mineral surface to the shear plane).

In (5) and (6), k_b is Boltzmann's constant, T is temperature (in K), ϵ_0 is the dielectric permittivity in vacuum, ϵ_r is the relative permittivity, e is the elementary charge, N is Avogadro's number, pH is the fluid pH, K_{Me} is the binding constant for sodium adsorption, $K_{(-)}$ is the disassociation constant for dehydrogenization of silanol surface sites, Γ_s is the surface site density, K_w is the disassociation constant of water, and C_f is the electrolyte concentration.

2.3. Surface Conduction. The surface conductance is calculated using the techniques described in [13, 28, 29] in which the surface conductance is given by

$$\Sigma_s = \Sigma_{\mathrm{EDL}} + \Sigma_{\mathrm{Stern}} + \Sigma_{\mathrm{Prot}}, \tag{8}$$

where Σ_{EDL}, Σ_{Stern}, and Σ_{Prot} are the contributions to the surface conductivity from ionic conduction in the EDL, in the Stern layer, and associated with proton transfer, respectively. Even the above formula is developed for 1 : 1 electrolyte of the aqueous NaCl solution and quartz; it still works for other porous materials such as Fontainebleau, Stainton, St. Bees sandstones, or Carbonates (see [13] for more details), where

$$\Sigma_{\mathrm{EDL}} = R\left\{\left[\left(\beta_{\mathrm{Na}^+}C_f + \beta_{\mathrm{H}+}10^{-\mathrm{pH}}\right) \times \left(\left(S\left(\frac{10^{-\mathrm{pH}} + K_M C_f}{2e\Gamma_s K_{(-)}}\right)\right)^{-1/3} - 1\right)\right] + \left[\left(\beta_{\mathrm{Cl}^-}C_f + \beta_{\mathrm{OH}^-}10^{\mathrm{pH}-pK_w}\right) \times \left(\left(S\left(\frac{10^{-\mathrm{pH}} + K_M C_f}{2e\Gamma_s K_{(-)}}\right)\right)^{+1/3} - 1\right)\right]\right\}, \tag{9}$$

$$\Sigma_{\mathrm{Stern}} = \frac{e\beta_s \Gamma_s k_M C_f}{10^{-\mathrm{pH}} + K_{(-)} + K_M C_f}, \tag{10}$$

$$\Sigma_{\mathrm{Prot}} = c_{\mathrm{Prot}}\Gamma_s, \tag{11}$$

in which $R = \sqrt{(2 \times 10^3 \epsilon_r \epsilon_0 k_b T N)/(C_f + 10^{-\mathrm{pH}})}$ and $S = \sqrt{8\ \times 10^3 \epsilon_r \epsilon_0 k_b T N (C_f + 10^{-\mathrm{pH}} + 10^{\mathrm{pH}-pK_w})}$. In (9)–(11) β_s is ionic Stern-plane mobility, β_{Na^+}, β_{H^+}, β_{Cl^-}, β_{OH^-} are ionic mobility of Na^+, ionic mobility of H+, ionic mobility of Cl^-, and ionic mobility of OH^- in the solution, respectively, and c_{Prot} is proton surface conductance.

2.4. Disassociation Constant. This parameter defines the fluid pH which is required to calculate the Stern potential and surface conductance. The value of K_w varies with temperature and is approximately in the range 0°C to 100°C as follows [30]:

$$K_w = 6.9978 \times 10^{-16} + 5.0178 \times 10^{-16}T - 2.4434 \times 10^{-17}T^2 + 7.1948 \times 10^{-19}T^3, \tag{12}$$

where T is in °C.

Indeed, the fluid pH is also defined by the reaction of water with carbon dioxide from the air which generates bicarbonate (HCO_3) and hydrogen ions (H^+) [13]. This leads to the fact that water that has been exposed to air is slightly acidic. In the model, one needs to know the pH to calculate the concentrations of hydrogen ions ($10^{-\mathrm{pH}}$) and hydroxyl ions ($10^{\mathrm{pH}-pK_w}$) in the fluid. The pH values required for the model are directly measured by a pH meter.

3. Experiments

Streaming Potential measurements have been performed on 20 consolidated samples (55 mm in length and 25 mm

Table 1: Sample ID, mineral compositions, and microstructure parameters of the samples. Symbols k_o (in mD), ϕ (in %), F (no units), α_∞ (no units), and ρ_s (in kg/m^3) stand for permeability, porosity, formation factor, tortuosity, and solid density, respectively. For lithology, EST stands for Estaillade limestone, IND stands for Indiana Limestone, BER and BereaUS stand for Berea sandstone, BEN stands for Bentheim sandstone, and DP stands for artificial ceramic core.

	Sample ID	Mineral compositions	k_o	ϕ	F	α_∞	ρ_s
1	EST	Mostly calcite (see [19])	294	31.5	9.0	2.8	2705
2	IND01	Mostly calcite, silica, alumina, and magnesium carbonate (see [20, 21])	103	20.0	32.0	6.4	2745
3	BER5	Silica (74.0–98.0%), alumina, and clays (see [21, 22])	51	21.1	14.5	3.1	2726
4	BER12	—	48	22.9	14.0	3.2	2775
5	BER502	—	182	22.5	13.5	3.0	2723
6	BER11	—	740	24.1	14.0	3.4	2679
7	BEN6	Mostly silica (see [23])	1382	22.3	12.0	2.7	2638
8	DP50	Alumina and fused silica (see http://www.tech-ceramics.co.uk/)	2960	48.5	4.2	2.0	3546
9	DP46i	—	4591	48.0	4.7	2.3	3559
10	DP217	—	370	45.4	4.5	2.0	3652
11	DP215	—	430	44.1	5.0	2.0	3453
12	DP43	—	4753	42.1	5.5	2.3	3373
13	DP172	—	5930	40.2	7.5	3.0	3258
14	BereaUS1	Silica, alumina, ferric oxide, and ferrous oxide (http://www.bereasandstonecores.com)	120	14.5	19.0	2.8	2602
15	BereaUS2	—	88	15.4	17.2	2.6	2576
16	BereaUS3	—	22	14.8	21.0	3.1	2711
17	BereaUS4	—	236	19.1	14.4	2.7	2617
18	BereaUS5	—	310	20.1	14.5	2.9	2514
19	BereaUS6	—	442	16.5	18.3	3.0	2541
20	BEN7	Mostly silica (see [23])	1438	22.2	12.6	2.8	2647

in diameter) including both natural and artificial samples from different sources (see Table 1). The natural samples numbered from 1 to 7 were obtained from Shell company [31]. Artificial samples numbered from 8 to 13 were obtained from HP Technical Ceramics Company in England. The natural samples numbered from 14 to 19 were obtained from Berea Sandstone Petroleum Cores Company in the USA. The last one numbered 20 was obtained from Delft University. The mineral compositions of all samples are also shown in Table 1.

The experimental setup for the Streaming Potential measurement as a function of concentration (at room temperature −22°C) as well as the method to measure the porosity, solid density, permeability, and formation factor is well described in [14]. For measuring the streaming potential as a function of temperature, we immersed the core holder and the bottle containing the solution into the bath of a thermally stabilized water bath (Thermo Fisher Scientific SC150 and A25) as shown in Figure 1.

The solutions used in our measurements were NaCl solutions with 7 different electrolyte concentrations (4.0×10^{-4} M, 1.0×10^{-3} M, 2.5×10^{-3} M, 5.0×10^{-3} M, 1.0×10^{-2} M, 2.0×10^{-2} M, and 5.0×10^{-2} M). Temperatures used in our measurements are 6°C, 11°C, 16°C, 16°C, 21°C, 26°C, 31°C, 36°C, 41°C, and 46°C, respectively. It should be noted that the model presented in Section 2 is valid in the range 0°C–100°C [13]. The solution was circulated through the samples until the electrical conductivity and pH of the solution reached a stable value. The pH values of equilibrium solutions are in the range 6.0 to 7.5 and the conductivities are saved for the zeta potential calculations. To avoid CO_2 uptake from the air that leads to change of conductivity and pH of the solutions, the solution container was tightly covered during experiment.

4. Results and Discussion

4.1. Porosity, Solid Density, Permeability, and Formation Factor. Porosity, density, and permeability of the samples are shown in Table 1 with an error of 3%, 5%, and 6%, respectively. Values of the formation factor and corresponding tortuosity are also reported in Table 1 with an error of 6% and 9%, respectively.

Table 2: The coupling coefficients (in mV/bar) for different concentrations of 4.0×10^{-4} M, 10^{-3} M, 2.5×10^{-3} M, 5.0×10^{-3} M, 10^{-2} M, 2.0×10^{-2} M, and 5.0×10^{-2} M, respectively.

Sample ID	0.4 mM	1 mM	2.5 mM	5 mM	10 mM	20 mM	50 mM
EST	−155.0	−86.0	−45.5	−23.0	−12.5	−6.8	−2.6
IND01	−68.0	−49.5	−25.0	−13.5	−7.6	−3.7	−1.8
BER5	−82.0	−56.0	−35.0	−21.0	−12.5	−7.0	−3.2
BER12	−94.0	−64.0	−36.0	−22.0	−13.0	−7.1	−3.3
BER502	−130.0	−85.0	−46.0	−24.5	−15.0	−8.5	−3.8
BER11	−180.0	−95.0	−55.0	−28.0	−17.0	−9.4	−4.4
BEN6	−480.0	−270.0	−105.0	−52.5	−27.0	−14.5	−6.1
DP50	−260.0	−155.0	−80.0	−45.0	−19.0	−8.4	−3.0
DP46i	−380.0	−210.0	−105.0	−53.0	−23.0	−12	−4.5
DP217	−280.0	−170.0	−85.0	−45.5	−24.0	−12.0	−4.6
DP215	−330.0	−190.0	−90.0	−56.0	−29.0	−14.0	−5.0
DP43	−390.0	−220.0	−78.0	−47.0	−22.0		
DP172	−510.0	−300.0	−96.0	−50.0	−28.0		
BereaUS1	−65.0	−45.0	−22.0	−17.5	−9.7	−6.0	−2.8
BereaUS2	−72.0	−50.0	32.5	−20.3	−12.0	−7.0	−3.3
BereaUS3	−44.0	−33.0	−22.5	−17.8	−9.8	−6.0	−2.9
BereaUS4	−130.0	−75.0	−45.0	−27.5	−14.0	−8.4	−4.1
BereaUS5	−155.0	−100.0	−49.0	−34.0	−17.0	−9.2	−4.4
BereaUS6	−75.0	−50.0	−25.0	−16.0	−6.4	−3.9	−2.0
BEN7	−550.0	−285.0	−110.0	−55.5	−28.0	−15.0	−6.7

4.2. Streaming Potential as a Function of Concentration. The way used to obtain the streaming coupling coefficients is the same as described in [14]. The streaming coupling coefficients at different solutions for all samples are shown in Table 2. It should be noted that experimental data for coupling coefficients of the samples numbered from 8 to 19 have been already published in [14]. There are no coupling coefficients for two samples DP43 and DP172 at concentrations of 2×10^{-2} M and 5×10^{-2} M because these samples are so permeable that they need a very large flow rate to generate measurable electric potentials at high concentration solutions. The maximum error of the coupling coefficients is 15%.

By using the input parameters presented by Glover et al. [13] in Table 3 except proton surface conductance c_{Prot} which is adjusted to fit data as described in [14], we have calculated the change of the zeta potential, the fluid viscosity, the relative permittivity, and the surface conduction against the electrolyte concentration.

According to Glover et al. [13], one can improve the fit of the model to the experimental data by introducing a constant zeta potential offset ζ_o. It means that (7) is replaced by $\zeta = \varphi_d \exp(-\chi_\zeta/\chi_d) + \zeta_o$. The zeta potential offset enables the model to reproduce the Streaming Potential coupling coefficient and zeta potential at high salinity. The physical meaning behind that is still unclear even though a possible explanation was partially given in [13]. Therefore, more research needs to be carried out to understand that parameter.

The relationship between the pore electrolyte concentration and fluid conductivity is now needed for the model. This relationship was found by fitting experimental data as shown, for example, in Figure 2 for the sample IND01. Figure 2 shows that the relationship follows $\sigma_f = 9.5C_f + 0.0085$ (S/m) for the sample IND01 and it is in good agreement with the model of Sen and Goode [32] for fluid conductivity of a NaCl solution as a function of electrolyte concentration in the ranges $10^{-6} < C_f < 1$ M and $15 < T < 25$°C ($\sigma_f = 10 C_f$). Similarly, the relationships between the pore electrolyte concentration and fluid conductivity were obtained for other samples.

All data is now sufficient to model the coupling coefficient as a function of electrolyte concentration with input

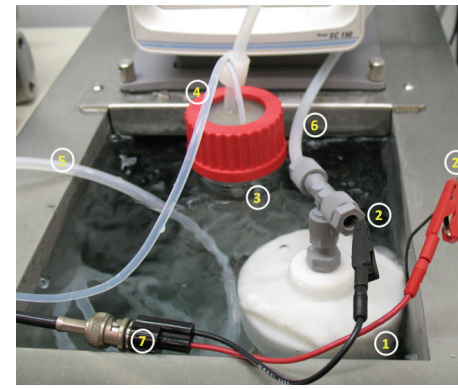

Figure 1: The main part of the setup for Streaming Potential measurements as a function of temperature. 1: core holder; 2: Ag/AgCl electrodes; 3: solution container; 4: tubing used to pump the solution from the container; 5: tubing connecting the pump outlet and the core holder inlet; 6: tubing for recirculation; 7: shield cable for electrical potential measurements.

Table 3: The parameters used in (5)–(12) of the model.

Parameter	Symbol	Value	Units
Temperature	T	6 to 46	°C
Electrolyte concentration	C_f	$(0.4–50) \times 10^{-3}$	mol/L
Fluid pH	pH	6 to 8	(—)
Dielectric permittivity in vacuum	ϵ_0	8.854×10^{-12}	F/m
Relative permittivity	ϵ_r	80	(—)
Boltzmann's constant	k_b	1.381×10^{-23}	J/K
Elementary charge	e	1.602×10^{-19}	C
Avogadro's number	N	6.022×10^{23}	/mol
Ionic mobility of Na^+ in solution	β_{Na^+}	5.20×10^{-8}	$m^2/s/V$
Ionic mobility of H^+ in solution	β_{H^+}	3.63×10^{-7}	$m^2/s/V$
Ionic mobility of Cl^- in solution	β_{Cl^-}	7.90×10^{-8}	$m^2/s/V$
Ionic mobility of OH^- in solution	β_{OH^-}	2.05×10^{-7}	$m^2/s/V$
Disassociation constant of water	K_w (22°C)	9.214×10^{-15}	(—)
Surface site density	Γ_s	10×10^{18}	Sites/m^2
Binding constant for sodium adsorption	K_{Me}	$10^{-7.5}$	(—)
Disassociation constant for dehydrogenization of silanol surface sites	$K_{(-)}$	$10^{-7.1}$	(—)
Proton surface conductance	c_{Prot}	$(2.8–12) \times 10^{-28}$	Sm^2/site
Ionic Stern-plane mobility	β_s	5.0×10^{-9}	$m^2/s/V$

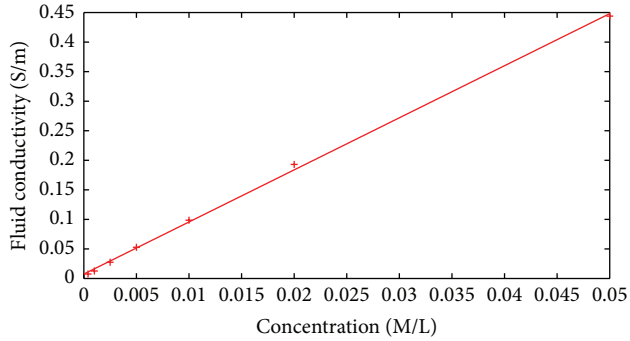

Figure 2: Fluid conductivity versus electrolyte concentration for sample IND01.

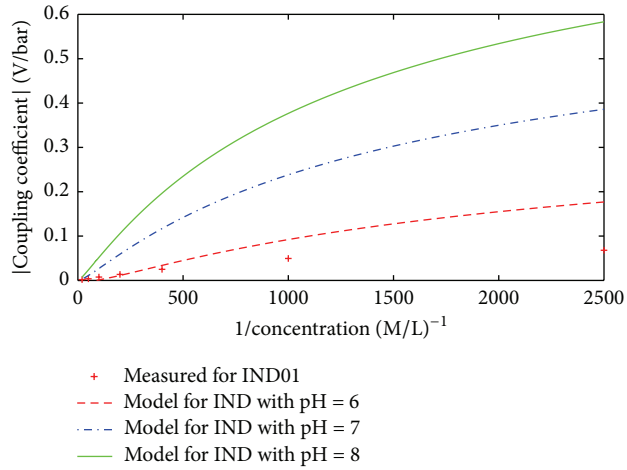

Figure 3: Measured and modeled results of the coupling coefficient for IND01. Three pH values (6, 7, and 8), the zeta potential offset (ζ_o = 0.045 V), and proton surface conductance $c_{Prot} = 3 \times 10^{-28}$ S m^2/site were used in the model.

parameters given by [13] in Table 3. Figure 3 shows the experimental and modeled results of Streaming Potential coupling coefficient for sample IND01. The modeled result was implemented for three values of pH (pH = 6, 7, and 8) with the zeta potential offset ζ_o = 0.045 V and the proton surface conductance $c_{Prot} = 3 \times 10^{-28}$ S m^2/site. Figure 3 shows that the model of coupling coefficient against the electrolyte concentration is very sensitive to the pH of the fluid as expected in [13]. The model is not in good agreement with the experimental result especially at a low concentration, where the deviation of coupling coefficient from experimental data becomes bigger.

The deviation between the modeled and experimental results could arise from the formula proposed to calculate the zeta potential in (5)–(7). According to the model, the zeta potential in magnitude would decrease drastically with increasing concentration as shown in Figure 4 (the solid line). However, based on the three measured coupling coefficients for all samples in Table 2 at high concentrations of 10^{-2} M, 2×10^{-2} M, and 5×10^{-2} M, the zeta potentials at those corresponding concentrations were calculated by using (2) as shown, for example, in Figure 4 (the dashed line) for sample US5. It is worthwhile noting that the surface conductance is neglected when the electrolyte concentration is higher than 10^{-2} M as mentioned in [14]. It is obvious that the

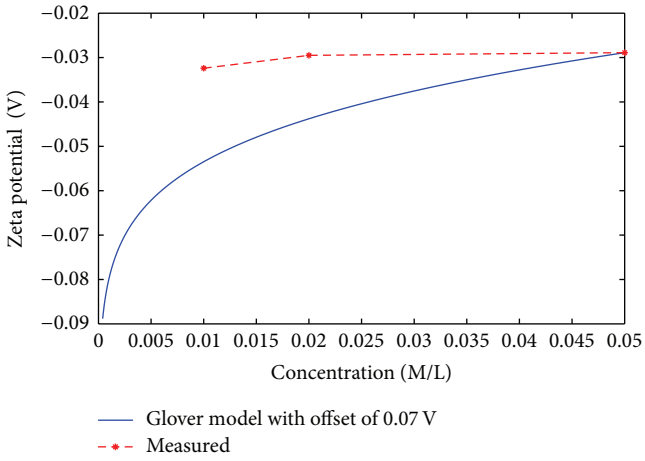

FIGURE 4: Zeta potential versus electrolyte concentration for sample BereaUS5.

measured zeta potential slightly decreases with increasing concentration and can be roughly considered constant over the studied range of the electrolyte concentration. Similarly, the zeta potentials were experimentally obtained for other samples.

We therefore assume the zeta potential to be constant over the electrolyte concentration and that is also inferred from the collected experimental data presented in [18]. The dependence of the coupling coefficient on the electrolyte concentration for all samples with corresponding proton surface conductance is experimentally and theoretically shown in Figure 5 in which Figure 5(a) is for the IND01 sample, Figure 5(b) is for the EST sample, Figure 5(c) is for the BEN6 and BEN7 samples, Figure 5(d) is for the set of BereaUS samples, Figure 5(e) is for the set of DP samples, and Figure 5(f) is for the set of BER samples, respectively. To avoid the overlap of the experimental data shown in Figures 5(d) and 5(e), we only show the experimental graphs for four out of six samples for the sets of BereaUS and DP samples, respectively. All theoretical results were carried out for pH of 6.7 because this value is the average of measured values (between 6 and 7.5). For reasons of clarity, the coupling coefficient is plotted against the reverse of electrolyte concentration rather than electrolyte concentration as shown in Figure 5. This is because we want to avoid the experimental data locating just on the bottom left corner of the graphs at low electrolyte concentrations.

Figure 5 shows that when the zeta potential is assumed to be constant over the electrolyte concentration, the model is well capable of producing the main features of the experimental data. It is also seen that the coupling coefficient is linearly proportional to the inverse of electrolyte concentration as expected at high concentrations when the surface conductance is ignored. This observation leads to the suggestion that the formula for the calculation of the zeta potential (see (4) to (7)) needs to be revised especially at a low concentration.

Due to the limitation of the model developed by Glover et al. [13] at low concentration, we have looked at other models to predict the streaming potential as a function of electrolyte concentration. For example, by fitting experimental data for quartz and NaCI or KCI at pH = 7 and $T = 25^{\circ}$C, Pride and Morgan [15] obtain the relation

$$\zeta = 8 + 26 \log 10 \left(C_f\right), \tag{13}$$

where ζ is in mV and C_f is the electrolyte concentration.

Similarly, Vinogradov et al. [16] obtain the relation between the zeta potential and electrolyte concentration based on published zeta potential data for quartz, silica, and glass in NaCl at pH = 6–8 as

$$\zeta = -9.67 + 19.02 \log 10 \left(C_f\right). \tag{14}$$

By fitting experimental data collected for sandstone, sand, silica nanochannels, Stainton, and Fontainebleau with electrolytes of NaCl and KCl at pH = 6–8, Jaafar et al. [17] obtain an empirical expression between the coupling coefficient and electrolyte concentration:

$$C_S = -1.36 {C_f}^{-0.9123}, \tag{15}$$

where C_S is expressed in mV MPa $^{-1}$.

Jouniaux and Ishido [18] obtains the other relations to predict the coupling coefficient from fluid conductivity based on numerous measurements of the streaming potential on sand with NaCl at pH = 7-8 which have been published:

$$C_S = \frac{-1.2 \times 10^{-8}}{\sigma_f}, \tag{16}$$

where σ_f is the fluid conductivity and C_S is in V Pa^{-1}.

Putting (13) and (14) into (3), the coupling coefficient as a function of electrolyte concentration (C_S-C_f) is obtained for the models of Pride and Morgan and Vinogradov et al., respectively. From (15), C_S-C_f is directly obtained for model of Jaafar et al. To plot C_S-C_f for the model of Jouniaux and Ishido from (16), the fluid conductivity as a function of electrolyte concentration obtained by fitting experimental data as shown in Figure 2 is used. The prediction of the coupling coefficient as a function of electrolyte concentration from all four empirical models is shown in Figure 6.

Because all empirical models are mostly obtained for the silica based samples, experimental data for Bentheim sandstone mainly made up by silica (see Table 1) are used for comparison as shown in Figure 6. The prediction from the model of Glover et al. with the adjustment of constant zeta potential for Bentheim sandstone shown in Figure 5(c) is also repeated in Figure 6. The comparison shows that all models converge and agree with the experimental data at high electrolyte concentration. However, at low concentration (smaller than 1.0×10^{-2} M) they diverge from each other and do not agree with measured data. Theoretical values from the models of Pride and Morgan as well as Vinogradov et al. are approximately twice as high as experimental values (see upper curves in Figure 6), while theoretical values from the models of Jouniaux and Ishido. are approximately half of the experimental values (see lower curves in Figure 6). Therefore, all four empirical models fail to predict the Streaming

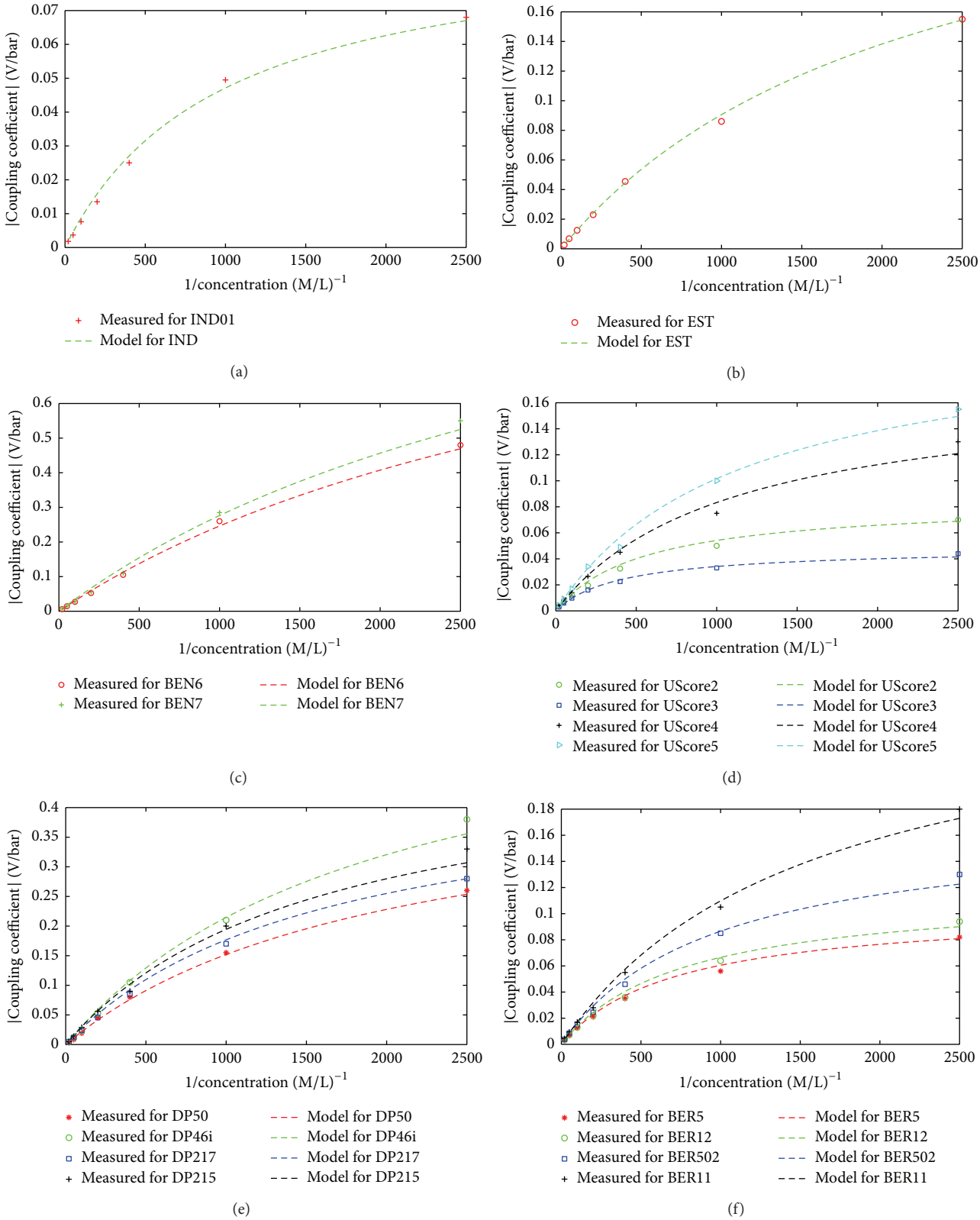

FIGURE 5: (a) is for the IND01 sample with $c_{\text{Prot}} = 3 \times 10^{-28}$ S m^2/site, (b) is for the EST sample with $c_{\text{Prot}} = 9.6 \times 10^{-28}$ S m^2/site, (c) is for the BEN6 and BEN7 samples with $c_{\text{Prot}} = 3 \times 10^{-28}$ S m^2/site, (d) is for the set of BereaUS samples with $c_{\text{Prot}} = 12 \times 10^{-28}$ S m^2/site, (e) is for the set of DP sample with $c_{\text{Prot}} = 3 \times 10^{-28}$ S m^2/site, and (f) is for the set of BER samples with $c_{\text{Prot}} = 3 \times 10^{-28}$ S m^2/site. The pH of 6.7 is used in the model for all samples.

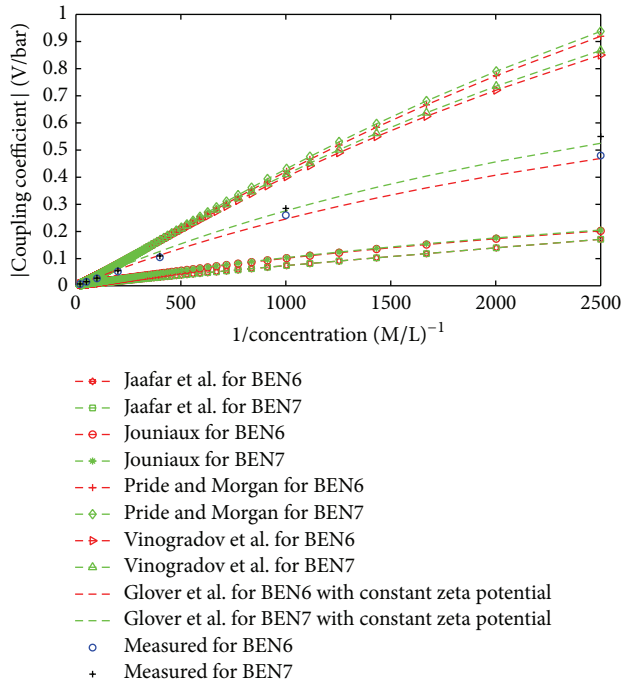

FIGURE 6: Coupling coefficient as a function of electrolyte concentration from different models.

Potential coupling coefficients as a function of the electrolyte concentration even for the most used materials such as silica and NaCl especially at low electrolyte concentrations. Figure 6 shows that the best approach to predict the coupling coefficient as a function of electrolyte concentration is to use the modified model of Glover et al. Besides four above models, there are also other ones available in literature, for example, from [26, 33, 34] that are not shown in Figure 6 due to the confusion.

4.3. Streaming Potential as a Function of Temperature. Measurement of the coupling coefficient as a function of temperature normally takes about 8 h for each sample. During that time, the coupling coefficient may change. To see how the coupling coefficient varies over time, we measured the coupling coefficient as a function of time at room temperature as shown in Figure 7(a) by continuously pumping the fluid through the sample and measuring the coupling coefficient after every fixed time interval. Figure 7 shows that firstly the coupling coefficient decreases drastically over time which could be due to the change of conductivity and pH (CO_2 uptake or electrode polarization drift or mineral decay from samples) and after about 40 h the coupling coefficient gets relatively stable. Therefore, the coupling coefficients as a function of temperature would be picked after 40 h.

To check how long it takes to get thermal equilibrium for the sample inside the core holder, we fixed a sensor probe tip of the digital temperature meter (Omega DP460) on the sample outlet surface and found that the time period to get thermal equilibrium is around 45 mins. Therefore, we take 45 mins as a time sampling (time between two consecutive measurements).

We also measured viscosity of the liquid as a function of temperature as shown in Figure 7(b) by comparing the slopes of flow rate-pressure difference straight lines (see [24]) at different temperatures to the reference slope at room temperature at which the fluid viscosity is known to be 0.96×10^{-3} Pa·s [35]. Figure 7(b) shows that the measured viscosities are in very good agreement with the model suggested by [35]. Therefore, the sample completely gets thermal equilibrium after 45 mins. To minimize the change of fluid conductivity over time, we used a solution of the relatively high concentration 5×10^{-3} M.

To model the coupling coefficient as a function of temperature, the same argument as described in Section 4.2 was used. The relative permittivity, viscosity, surface conductance, disassociation constant, and fluid conductivity at the concentration of 5×10^{-3} M as a function of temperature are theoretically given in [13]. The zeta-potential offset ζ_o was found by fitting the experimental data of the coupling coefficient for each sample. Figure 8 shows the experimental results and modeled results of coupling coefficient for sample IND01 in which three pH values (6, 7, and 8), three corresponding zeta-potential offsets (ζ_o = 0.045 V, 0.083 V, and 0.12 V), and proton surface conductance $c_{\text{Prot}} = 3 \times 10^{-28}$ S m^2/site were used to model. It was seen that the coupling coefficient versus temperature is also very sensitive to fluid pH and pH = 6 gives better fit than the others. Therefore, pH = 6 was used to model the coupling coefficient versus temperature for representative samples of EST, BereaUS5, DP217, and BER502 as shown in Figure 9. Both the experimental and theoretical results show that the coupling coefficient increases with increasing temperature. However, Figure 9 shows an essential deviation between experimental data and the model. The origin of that deviation is still unclear. One of the reasons may be due to a temperature activated transport process happening around 300 K, which obviously cannot be explained by the model and needs to be explored.

5. Conclusion

We have measured Streaming Potential coupling coefficients for 20 consolidated samples with 7 different concentration NaCl solutions and 9 different temperatures under well-controlled conditions (pH, temperature, and quality of distilled water). Afterwards the model has been used by taking fluid parameters, rock-fluid interface parameters already provided in [13], and rock microstructure parameters (porosity, permeability, and formation factor) measured by us for all the samples. The proton surface conductance was adjusted to fit the experimental data. The comparisons were carried out for each sample.

For concentration dependence of the coupling coefficient, the comparison shows that the theoretical model is not in agreement with the experimental data, especially in the low concentration range. However, if the zeta potential is considered to be constant over a small range of electrolyte concentrations the model fits the experimental data very well.

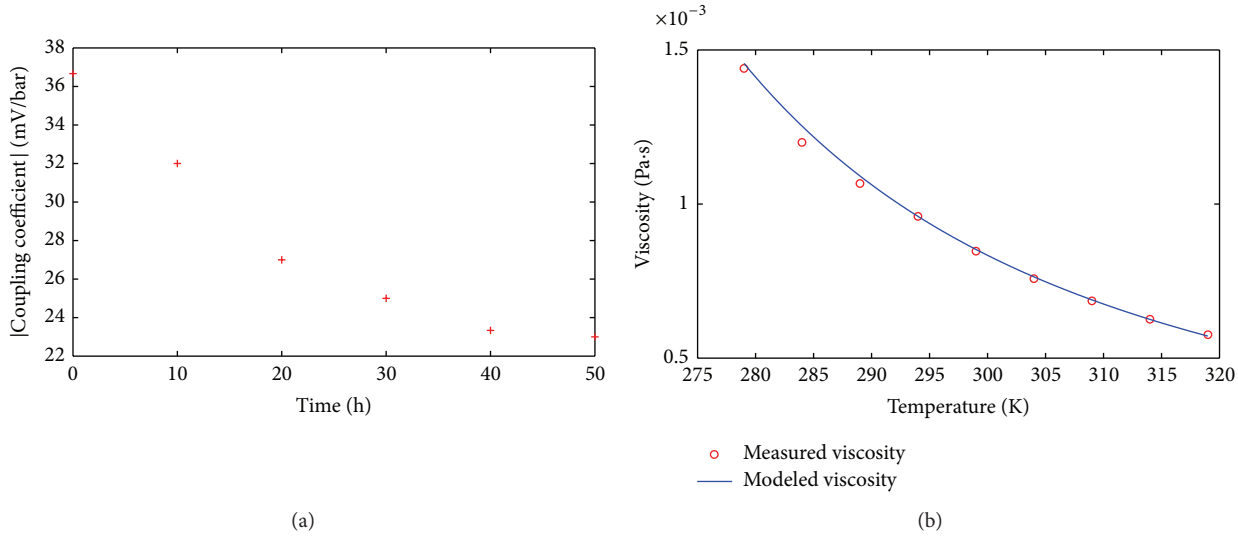

FIGURE 7: (a) $|C_S|$ versus time at room temperature for sample BereaUS5 and 5×10^{-3} M. (b) The relationship between viscosity and temperature.

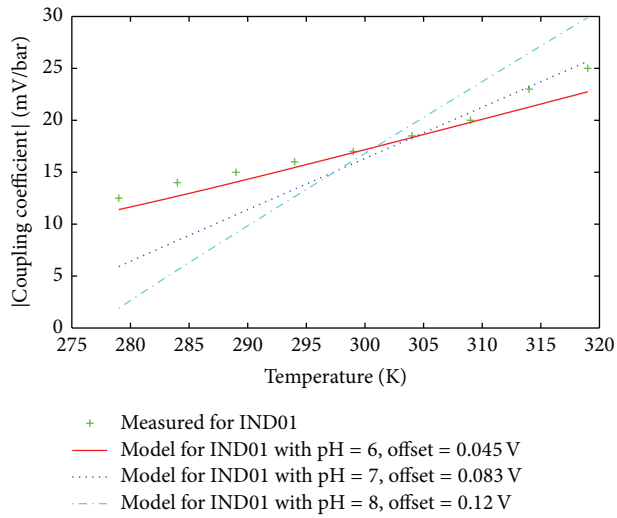

FIGURE 8: Measured and modeled coupling coefficient as a function of temperature at 5×10^{-3} M for sample IND01. Three pH values (6, 7, and 8), three corresponding zeta potential offsets (ζ_o = 0.045 V, 0.083 V, and 0.12 V), and proton surface conductance $c_{\text{Prot}} = 3 \times 10^{-28}$ S m^2/site were used in the model.

This leads to the suggestion that the formula of the zeta potential against electrolyte concentration presented in the model needs to be recalculated and adjusted accordingly. Besides the model given in [13], we also use other models to predict the streaming potential as a function of electrolyte concentration. But none of them can fit the experimental data at low electrolyte concentration. Therefore, further revisions of those models need to be carried out for a better fit at low electrolyte concentration. Of all the models used for the comparison, the modified model of Glover et al. with assuming of constant zeta potential that is experimentally measured is the best approach to predict the coupling coefficient as a function of electrolyte concentration.

For temperature dependence of the coupling coefficient, we implemented a zeta-potential offset to the model which improves the fit to experimental data. The comparison shows that the theoretical model does not fit the experimental data well, but it can show the increase of coupling coefficient with increasing temperature as measured. The reason for that could be due to the variation of the input parameters over temperature because the Streaming Potential coefficient is sensitive to changes in the input parameters that describe the rock-fluid interface, such as the surface site density (Γ_s), the binding constant (K_{Me}), and the disassociation constant ($K_{(-)}$) [13]. Therefore, more research about the change of the input parameters versus temperature needs to be conducted for a better explanation. A possible explanation of the deviation at around 300 K could be a temperature activated transport process. The results also show that the model is very sensitive to the pH of the pore fluid, especially for the Streaming Potential coefficient as a function of temperature. So the fluid pH needs to be carefully taken into account during measurements.

Conflict of Interests

The authors declare that there is no conflict of interests regarding the publication of this paper.

Acknowledgments

This work was partly funded by Shell Oil Company and the Foundation for Fundamental Research on Matter (FOM) in The Netherlands in the program for "Innovative physics for oil and gas." The authors would also like to thank Boris N. Kuvshinov (Shell) and Karel Heller (TU Delft) for providing them with the samples used in the experiments and Hans

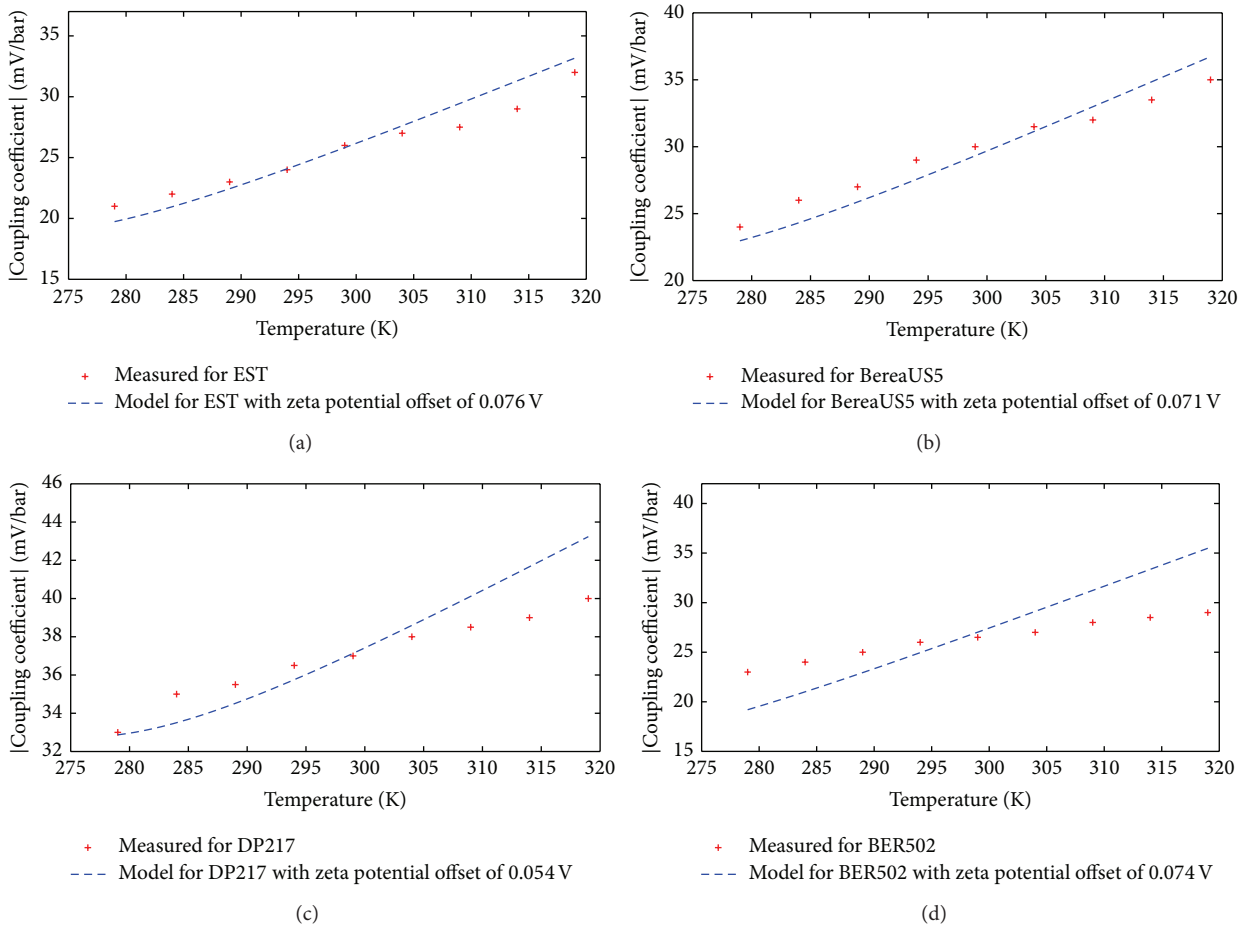

FIGURE 9: (a) is for the EST sample, (b) is for the BereaUS5 sample, (c) is for the DP217 sample, and (d) is for the BER502 sample.

Ellermeijer for his assistance in building up the experimental setups.

References

[1] B. Wurmstich and F. D. Morgan, "Modeling of streaming potential responses caused by oil well pumping," *Geophysics*, vol. 59, no. 1, pp. 46–56, 1994.

[2] R. F. Corwin and D. B. Hoover, "Self-potential method in geothermal exploration," *Geophysics*, vol. 44, no. 2, pp. 226–245, 1979.

[3] F. D. Morgan, E. R. Williams, and T. R. Madden, "Streaming potential properties of Westerly granite with applications," *Journal of Geophysical Research*, vol. 94, no. 9, pp. 12–461, 1989.

[4] A. Revil and P. A. Pezard, "Streaming electrical potential anomaly along faults in geothermal areas," *Geophysical Research Letters*, vol. 25, no. 16, pp. 3197–3200, 1998.

[5] H. Mizutani, T. Ishido, T. Yokokura, and S. Ohnishi, "Electrokinetic phenomena associated with earthquakes," *Geophysical Research Letters*, vol. 3, no. 7, pp. 365–368, 1976.

[6] M. Trique, P. Richon, F. Perrier, J. P. Avouac, and J. C. Sabroux, "Radon emanation and electric potential variations associated with transient deformation near reservoir lakes," *Nature*, vol. 399, no. 6732, pp. 137–141, 1999.

[7] A. Thompson, S. Hornbostel, J. Burns et al., "Waveform design for electroseismic exploration," in *SEG Technical Program Expanded Abstracts*, pp. 557–560, 2005.

[8] S. S. Haines, A. Guitton, and B. Biondi, "Seismoelectric data processing for surface surveys of shallow targets," *Geophysics*, vol. 72, no. 2, pp. G1–G8, 2007.

[9] M. Strahser, L. Jouniaux, P. Sailhac, P. D. Matthey, and M. Zillmer, "Dependence of seismoelectric amplitudes on water content," *Geophysical Journal International*, vol. 187, no. 3, pp. 1378–1392, 2011.

[10] S. Garambois and M. Dietrich, "Seismoelectric wave conversions in porous media: field measurements and transfer function analysis," *Geophysics*, vol. 66, no. 5, pp. 1417–1430, 2001.

[11] P. W. J. Glover and M. D. Jackson, "Borehole electrokinetics," *Leading Edge*, vol. 29, no. 6, pp. 724–728, 2010.

[12] S. Pride, "Governing equations for the coupled electromagnetics and acoustics of porous media," *Physical Review B*, vol. 50, no. 21, pp. 15678–15696, 1994.

[13] P. W. J. Glover, E. Walker, and M. D. Jackson, "Streaming-potential coefficient of reservoir rock: a theoretical model," *Geophysics*, vol. 77, no. 2, pp. D17–D43, 2012.

[14] D. T. Luong and R. Sprik, "Permeability dependence of Streaming potential coupling coefficient," Submitted to *Geophysics*.

[15] S. R. Pride and F. D. Morgan, "Electrokinetic dissipation induced by seismic waves," *Geophysics*, vol. 56, no. 7, pp. 914–925, 1991.

[16] J. Vinogradov, M. Z. Jaafar, and M. D. Jackson, "Measurement of streaming potential coupling coefficient in sandstones saturated with natural and artificial brines at high salinity," *Journal of Geophysical Research B: Solid Earth*, vol. 115, no. 12, Article ID B12204, 2010.

[17] M. Z. Jaafar, J. Vinogradov, and M. D. Jackson, "Measurement of streaming potential coupling coefficient in sandstones saturated with high salinity NaCl brine," *Geophysical Research Letters*, vol. 36, no. 21, Article ID L21306, 2009.

[18] L. Jouniaux and T. Ishido, "Electrokinetics in earth sciences: a tutorial," *International Journal of Geophysics*, vol. 2012, Article ID 286107, 16 pages, 2012.

[19] E. Bemer, O. Vincké, and P. Longuemare, "Geomechanical log deduced from porosity and mineralogical content," *Oil and Gas Science and Technology*, vol. 59, no. 4, pp. 405–426, 2004.

[20] I. T. Committee, *Indiana Limestone Handbook*, Indiana Limestone Institute of America, 2007.

[21] P. Churcher, P. French, J. Shaw, and L. Schramm, "Rock properties of Berea sandstone, Baker dolomite, and Indiana limestone," in *Proceedings of the SPE International Symposium on Oilfield Chemistry*, February 1991.

[22] A. Pagoulatos, *Evaluation of multistage triaxial testing on Berea sandstone [M.S. thesis]*, University of Oklahoma, Norman, Okla, USA, 2004.

[23] A. A. Tchistiakov, "Physico-chemical aspects of clay migration and injectivity decrease of geothermal classic reservoirs," in *Proceedings of the World Geothermal Congress*, pp. 3087–3095, May 2000.

[24] D. T. Luong and R. Sprik, "Streaming potential and electroosmosis measurements to characterize porous materials," *ISRN Geophysics*, vol. 2013, Article ID 496352, 8 pages, 2013.

[25] L. Jouniaux, M. L. Bernard, M. Zamora, and J. P. Pozzi, "Streaming potential in volcanic rocks from Mount Pelée," *Journal of Geophysical Research B: Solid Earth*, vol. 105, no. 4, pp. 8391–8401, 2000.

[26] A. Bolève, A. Crespy, A. Revil, F. Janod, and J. L. Mattiuzzo, "Streaming potentials of granular media: influence of the Dukhin and Reynolds numbers," *Journal of Geophysical Research B: Solid Earth*, vol. 112, no. 8, Article ID B08204, 2007.

[27] R. J. Hunter, *Zeta Potential in Colloid Science*, Academic Press, New York, NY, USA, 1981.

[28] A. Revil and P. W. J. Glover, "Theory of ionic-surface electrical conduction in porous media," *Physical Review B*, vol. 55, pp. 1757–1773, 1997.

[29] A. Revil, P. A. Pezard, and P. W. J. Glover, "Streaming potential in porous media 1. Theory of the zeta potential," *Journal of Geophysical Research B: Solid Earth*, vol. 104, no. 9, pp. 20021–20031, 1999.

[30] D. R. Lide, *CRC Handbook of Chemistry and Physics*, CRC Press, 2004.

[31] B. N. Kuvshinov, *Shell International Exploration and Production*, B.V. Company, InformationRijswijk, The Netherlands, 2012.

[32] P. N. Sen and P. A. Goode, "Influence of temperature on electrical conductivity on shaly sands," *Geophysics*, vol. 57, no. 1, pp. 89–96, 1992.

[33] P. R. Johnson, "A comparison of streaming and microelectrophoresis methods for obtaining the ζ potential of granular porous media surfaces," *Journal of Colloid and Interface Science*, vol. 209, no. 1, pp. 264–267, 1999.

[34] B. J. Kirby and E. F. Hasselbrink Jr., "Zeta potential of microfluidic substrates. 1: theory, experimental techniques, and effects on separations," *Electrophoresis*, vol. 25, no. 2, pp. 187–202, 2004.

[35] S. L. Phillips, H. Ozbek, and R. Otto, "Basic energy properties of electrolytic solutions database," in *Proceedings of the 6th International CODATA Conference*, May 1978.